E-ISSN: 2997-9382

SemantJournals

American Journal of Technology Advancement

https://semantjournals.org/index.php/AJTA

| Research Article

Check for updates

Optical Properties of Nanotechnology Based on Image Sensors

Ayad Mohammed Abdulla, Bassam Mohsen Atiyah

Electronic Department, Kirkuk Technical Institute, Northern Technical University, Kirkuk, Iraq

ayad-mohammed@ntu.edu.iq, Bassam201214@ntu.edu.iq

Annotation

Advanced plasmonic color filters for cutting-edge silicon complementary metal oxide semiconductor image sensors are the focus of this study, which also delves into the optical characteristics of plasmonic hole arrays. The aperture arrays are carefully engineered to function at the principal red, green, and blue colors; they consist of subwavelength-sized holes arranged in a hexagonal pattern on a 200 nm aluminum sheet. Transmission peaks may be seen in plasmonic filters with large hole arrays (>6 x 6 μm²) ranging from 40% to 60%. These filters continue to handle data for pixels as small as 1 × 1 μm², but they compromise transmission efficiency in the process. The filtering function of hole array filters is maintained even when random defects are present, and they are resilient to the spatial communication between pixels that are inside our detection limit. According to research on filter transmittance and crosstalk, the transmission properties of plasmonic hole array filters are mostly influenced by interactions between closest neighboring holes, rather than by long-range interactions. Additional evidence for this comes from a simple nearest neighbor model that, given a number of holes, reliably predicts the transmission efficiency of the hole array.

Keywords: transmission qualities, image sensors, primary hues.

1. INTRODUCTION

Metal films with periodic hole arrays of subwavelength dimensions are acknowledged for their capacity to serve as optical filters owing to the interference generated by the surface.

(SPPs) across adjacent apertures. Plasmonic filters, unlike current on-chip organic color filters, have enhanced color tunability due to the use of a single perforated metal layer. Moreover, these filters are impervious to performance loss caused by ultraviolet (UV) light [1]. To attain effective on-chip integration, it is essential that the plasmonic filter exhibits the following attributes: compatibility with contemporary image sensors featuring extensive functional array sizes and diminutive (1 × 1 μm²) pixel dimensions, as well as resilience to random defects and spatial crosstalk-color effects [2]. Various research teams have performed extensive studies on the phenomena to enhance transmission through optically thick metal sheets with arrays of subwavelength-sized apertures. The increased The creation of surface plasmon polaritons on the metal's surface might be the explanation for the transmission seen in hole arrays. Upon activation

at each hole, these SPPs communicate with one another across neighboring holes.. Transmission improvements are found at core frequencies dictated by the physical size of the apertures, the thickness of the metal layer, and the dielectric medium And optical properties of the metal and Hole array films have attracted significant attention owing to their estimated peak transmission efficiencies over 20% at visible wavelengths, making them intriguing candidates for use as spectral filters in imaging technologies [5] [6]. In modern image sensor technologies, Photo detective pixels in various integrated circuits, such as complementary metal oxide semiconductor image sensors (CISs) and charge-coupled devices (CCDs) and, have their color sensitivity improved by the addition of on-chip color filters (OCCFs). It is common practice to use the organic dyes linked with the three primary colors when crafting such organic color palettes.

Conversely, organic dye filters have limited resistance to high temperatures and extended exposure to elevated amounts of UV light. Furthermore, due to the dye compound's low absorption coefficient, their thickness is restricted to a maximum of few hundred nanometers.

all circumstances. After precisely aligning lithography of each color filter type throughout the whole photodiode array, the manufacturing of the three organic dye filters for a amber/magenta/cyan or blue/green/red color scheme is required in order to carry out the process. In order to accomplish the color scheme that you have in mind, this is vital. Because of this, it is hard to construct multicolor imaging systems that have both large array formats and extremely minute pixels. This may be a significant limitation. At the other end of the spectrum, The physical design largely dictates the transmission qualities of periodic hole array plasmonic metal filters. It is possible to regulate the aperture array's transmission spectrum.

by the use of a single thin sheet of metal, which is a practical option. Modifying the apertures in terms of their size, configuration, and distance from one another is one way to do this kind of thing. As a result of this property, plasmonic color filters are exceptional in terms of cost-effectiveness, especially for applications that include imaging in a number of different hues. Plasmonic filters, in comparison to traditional filters, provide a variety of extra advantages that are not accessible with conventional filters. These benefits include the ability to save time and money. A variety of benefits are available, some of which include increased reliability in the face of prolonged exposure to ultraviolet radiation, as well as rising temperatures and humidity over extended periods of time [9]. Some of these benefits are listed below. In light of recent findings that have led to the integration of a plasmonic hole array color filter into a complementary metal oxide semiconductor image sensor, this integration has been made possible as a result of these discoveries. Because of this, the capabilities of visible filtering have been made available to be shown. On the other hand, the majority of the focus of prior research has been on the transmission characteristics of large filters, whereas important filter performance features that are needed for cutting-edge image sensor applications have been neglected. The influence of filter transmission on spatial color array size, resistance, , and crosstalk to defects are some of the factors that are included in this discussion [10].

2. METHODOLOGY

These are the optical properties of hexagonal arrays with subwavelength holes that are formed of aluminum sheets with a thickness of 250 nanometers. Which are suitable for incorporation into image sensors, are examined in this work. There is an extensive description of the optical characteristics [11]. We employed a 20 kV, 15 pA In order to construct hole array filters for our experiments, we utilized a focused ion beam to mill the appropriate hole array patterns onto an evaporated aluminum film with a thickness of 250 nanometers. This film was then put on square quartz substrates of one inch in size. We build separate square filters with 15 × 15 holes that were hexagonally aligned in order to study the connection between the transmission of a hole array and the period and diameter of visible wavelengths. There was some variation in the hole diameter (d)

from 70 to 380 nm in 30 nm increments, while the period (p) spanned 200 to 520 nm in 30 nm increments.

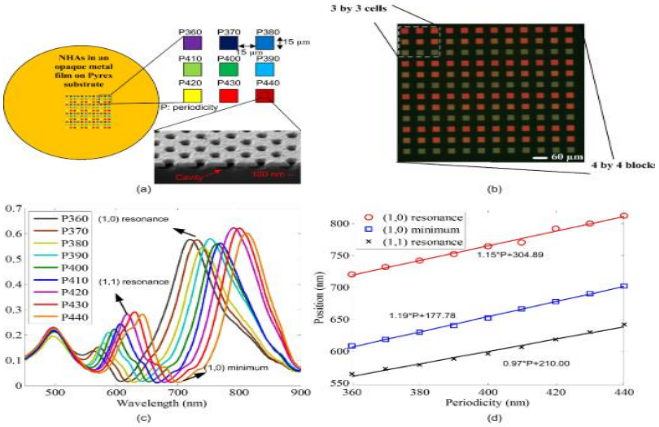

Figure 1: (a) scope images of the productid hole array filters under back illumination. Every filter is composed of arrays of 14 × 14 hexagonally packed holes. (b) The scanning electron micrograph showed a typical hole array filter with 14 × 14 holes that were hexagonally aligned, with dimensions of 200 nm in length and 310 nm in width. (c) a shade of green with a wavelength of 160–200 nm and a protein concentration of 320 nm. the color red, with a wavelength of 110 to 250 nanometers and a wavelength of 240 nanometers The dotted lines indicate the blue light spectra (p = 250 nm, d = 101−160 nm), whilst the solid lines reflect the simulated spectra. You can see that all three color spectrum are represented by a 30 nanometer increment in pore diameter.

Incident light that passed through a conversion filter producing blackbody emission much like the sun (5400 K in color temperature). For incident light to be collimated, both the aperture stop and field diaphragm of the microscope were closed. The spectroscopy apparatus was used to collect all filter spectra. CCD detector with a resolution of 1240 by 130 pixels and a sensitivity in the 320–820 nm range was employed to measure the spectra. Absolute transmission of To find each filter, we divided the transmission spectra of the hole array filters by the spectra of the open apertures of the same size.. Throughout characterization, the open window spectra were measured hourly to ensure the stability of the measurement system [12].

3. STEPS OF FABRICATION

The fabricated hole array filters are depicted in Figure 1a as seen through a back-illuminated microscope. Each filter is composed of arrays of 15× 15 holes, with hole diameters ranging from 80 to 280 nm and hole periods spanning from 210 to 400 nm from left to right. The 300 nm period filters have a spatial resolution of approximately 2.5 μm × 2.0 μm, while the 400 nm period filters have a resolution of approximately 6.0 μm × 7.9 μm. SEM image of a representative filter with d = 250 nm and p = 320 nm is depicted in the inset image (Figure 1b). Each of the panels in Figure 1c and 1d displays the transmission spectra that were measured for the hole array periodicities that were associated with a distinct diameter. The green panel (p = 330 nm), the blue panel (p = 250 nm), and the red panel (p = 320 nm) each have their own unique diameter. The color-dotted lines in the observed spectra suggest it shifts to longer wavelengths at the peak transmission point as the hole period increases. Proof of this may be seen in the fact that, simultaneously, the peak transmission efficiency increases as the hole diameter increases. In the visible spectrum, the spectral full-width half-maximum (fwhm) is roughly 250 nanometers, which equates to a maximal transmission of sixty to seventy percent. For the purpose of validating the spectra that were obtained, three-dimensional full-field electromagnetic simulations were used to mimic the transmission response of the filter that was manufactured. An aperture with the same pitch and

diameter is incorporated in the SiO2 matrix of the simulation model, and it is perforated with hexagonally aligned apertures. The produced aluminum film is perforated with these apertures.

150 nanometers is the thickness of the aluminum film. Through the use of a broadband planewave source that emits at normal incidence, the optical response of the hole array film that is produced is stimulated throughout the wavelength range of 300 to 900 nanometers. A representation of the simulated transmission spectra can be seen in Figure 1c and 1d in the form of red solid lines. The only major variation between the simulated and measured spectra is the presence of broad profiles, which may be indicative of manufacturing faults for example, the the Al film's surface roughness or synthetic profiles. The measured spectra are mostly consistent with the simulated profiles.

The red color filter designs do, however, display a little unwanted transmission in the blue spectral region, even though they provide vibrant colors and demonstrate impressive peak transmission efficiency across the visible spectrum. Crosstalk occurs between the blue component of the spectrum and the red color filters (p = 320−400 nm, d > 100 nm). These filters were intended to maximize transmission in the 400−700 nm range ($\lambda 0 < 400$ nm), and the blue section of the spectrum becomes affected by this crosstalk. Evidently, this is the case from Figure 1. As a result of this undesirable transmission, as is seen in Figure 1a, the red color filters have a little but noticeable appearance of pink, magenta, and violet. Although signal processing may easily resolve spectral crosstalk, optimal RGB filters are not necessary for imaging applications. This is an essential point to emphasize since it ought to be brought to your attention. In spite of this, we made use of full-field simulations in order to portray the spectrally resolved electric field distribution parallel to the polarization of the incoming planewave along the diameter of the perforations. This was done in order to get a better understanding of the genesis of the spectral crosstalk.

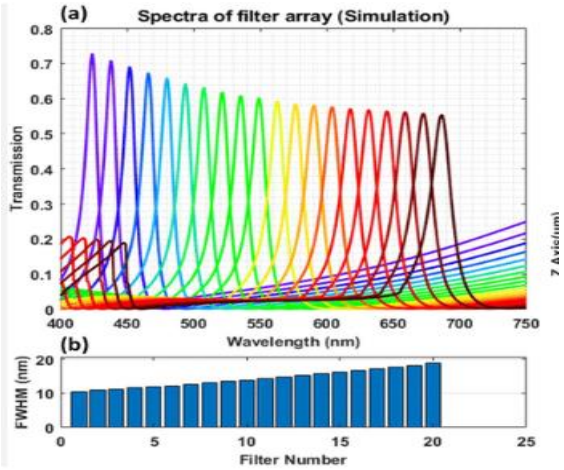

Figure 2: With p = 300 nm and d = 200 nm optimized, the simulations show that the hole array filter transmits red light.

The dispersion of electric fields at the targeted wavelengths is, in contrast to the plane wave used to excite the structure, illustrated in the upper four panels along the diameter of the apertures.

Included in the figure is the blue element's simulated transmission profile as well as the cross-sectional electric field distributions at several appropriate wavelengths. The simulated spectrum displays two broad transmission bands, which are in agreement with our measurements. These bands are separated by a null point at 520 nm, which is inherent to the hexagonally aligned hole array structure's reciprocal lattice vector. The longer wavelength transmission band exhibits transmission peaks at 543 and 652 nm, which are indicative of a highly localized electric field, as determined by the electric field intensity maps.

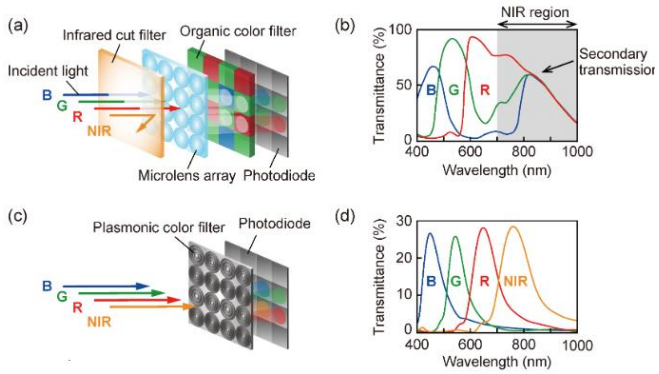

Figure 3: The transmission spectra of hole array filters optimized to detect certain wavelengths (d = 250 nm for green, p = 320 nm for blue, p = 350 nm for red, and d = 160 nm for green and 260 nm, respectively) for these colors were obtained using filters of the following dimensions: (a) 9 µm-, (b) 7µm-, (c) 3.2 µm² and 4.4 µm². The insets of panels a-d depict back-illuminated microscopic photographs of the filter, with corresponding fields of view of 3.0 µm-squared, 13 µm-squared, 6.5 µm-squared, and 5.0 µm The corresponding SEM images are rendered using RGB filters with a dimension of 6.2 µm. Letters of Nano Scale

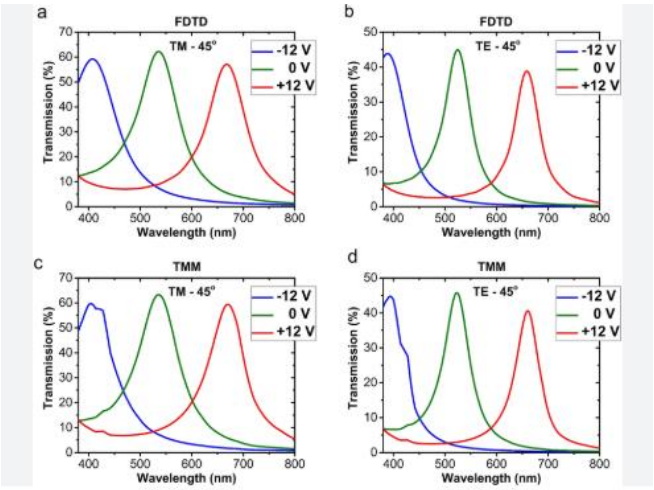

Figure 4: Color filter pairs having no distinction in their sliced transmission spectra. a) A typical scanning electron micrograph showing the border between two of these filters.

The color filter pairs were photographed using a color CCD camera and the photos were captured using a back-illuminated microscope.

The white lines represent scale bars that are 30 µm in size. wide region conducted at the sites indicated by the green ticks in (b)

is used to capture the spectra of each color filter pair. The sliced spectra for the red/green , green/blue and blue/red filter pairings are shown in (e), (g), and (i), respectively.

4. CIRCUIT PROPERTIES

We gather spectra from three distinct sets of color filter pair R/G, G/B and B/R in order to explore the impacts of color crosstalk between neighboring pixels. These sets of color filter pairs are B/R, G/B, and R/G. A 9 × 17 µm2 array is included in every set. These sets are comprised of a variety of color combinations, and there is no space between them. Figure 4b–d depicts backlit views of the filter pairs, while Figure 4a displays a characteristic scanning electron micrograph of the border between two of these hole array filters. Both of these images are shown in the same figure.

It can be seen in Figure 4e that the measured Each individual sliced spectra shown in Figure 4b represents an integrated cross-sectional area that is 2 micrometers in width and is taken perpendicular to the filter pair border. The yellow ticks on the spectrum reflect the locations of these sections. The complementary spectra of the other two filter color combinations are shown in Figure 4i for your viewing pleasure. One of the panels that illustrates the correlation function Δi, which is a measurement of the difference between each sliced spectrum, is seen in Figure 4f.

$$\Delta_i = \alpha_i \int_{\lambda_{min}}^{\lambda_{max}} (T_1(\lambda) - T_{G,R}) \, d\nu \qquad 1$$

Δi may range from 1 to 2, where α_i represents a constant that acts as a normalizer for each spectrum that is measured, and its value is determined by the correlation that exists between the measured spectrum and the averaged spectrum. It is shown that the correlation functions depicted in Figure 4h, f, and e experience an inversion when they move from one color filter to another.

It is possible to make an estimate based on these graphs that there is a spatial color crosstalk between the filters that is as small as 2 micrometers. Due to the fact that this length include both the diffraction limit and some defocus from the measurement parameters, there is a potential that the crosstalk across filters is virtually identical to our detection limit. It is important to observe that although though the filters are not separated in any manner, Figure 4c–e clearly displays dark lines linking pairs of filters, which suggests that there is a moderate amount of spatial color crosstalk between them. In light of the fact that manufacturing errors are inescapable, it is of the utmost importance to acknowledge the influence that random imperfections have on the transmission and spectral shape of filters. We conducted a series of tests to determine the durability of the hole array filter design. These tests included testing the transmission of 22 × 22 green filters with randomly located absent apertures. The density of the filters was 5, 10, 20, 30, and 40%. As shown in Figure 5a, the resulting spectra demonstrate that the shape and efficiency of the filter transmission remain unchanged when the random defect densities are less than or equal to 7%. On the other hand, the filter transmission decreases in a monotonic manner when the random defect densities are more than or equal to 12%. In spite of this, when we compare the spectra by utilizing their peak transmissions, as shown in Figure 5ab, we find that regardless of the number of filter faults, all of the spectra display line forms that are essentially similar to one another. It may be deduced from this that the presence of random faults has an effect only on the effectiveness of the filter transmissions, and not on the spectral form.

In Figure 4c, we provide the relative peak transmission efficiency in comparison to the random defect density. It is clear from this plot that the relationship is not linear, which suggests that the decrease in transmission efficiency that occurs with a rise in defect density is not just the result of a geometrical impact as previously thought. For the purpose of gaining an understanding of the optical processes that are responsible for controlling this pattern, we provide a fundamental analytical model that characterizes the effectiveness of transmission from hole arrays by using interactions with their respective nearest neighbors.

5. CONCLUSIONS

Plasmonic hole array color filters allow one sheet of perforated metal to be used to control over the visible spectrum. These filters provide a great substitute when weighed against the traditional on-chip dielectric filters utilized in semiconductor manufacture. This is particularly true for visually appealing correspondence with a range of colors. Our results show that hole array filters' transmission properties are unaffected by random flaws , spatial crosstalk and array size from neighboring filters of different colors. Therefore, our case proves this. Because of this, interactions with nearby neighbors are the primary means of determining the scattering dynamics

of hole array filters. Because of its restricted number of holes and its limitations in spatial crosstalk and light-filtering capabilities, the hole array is a good choice for applications that need very tightly packed filtering components in two-dimensional image sensors.

This is related to the hole diameters. Their filtering capacity, which is both long-lasting and strong, makes them also perfect. Their resistance to random flaws makes them common targets for industrial bulk manufacture. Having said that, the field of plasmonic filters will need additional technical innovations. More research is needed, particularly on the integration of a filter into a complementary metal oxide semiconductor image sensor, thereby enabling the use of this technology in industry. prove their relevance, dependability, and benefits over more traditional methods.

6. REFERENCES

1. Bigdeli, Arafeh, et al. "Nanoparticle-based optical sensor arrays." *Nanoscale* 9.43 (2017): 16546-16563.
2. Zhang, Jin Zhong. *Optical properties and spectroscopy of nanomaterials*. World Scientific, 2009.
3. Ray, Paresh Chandra. "Size and shape dependent second order nonlinear optical properties of nanomaterials and their application in biological and chemical sensing." *Chemical reviews* 110.9 (2010): 5332-5365.
4. Hassan, Dilawar, et al. "Fluorescent nanotechnology: An evolution in optical sensors." *Current Analytical Chemistry* 18.2 (2022): 176-185.
5. Jain, Prashant K., et al. "Noble metals on the nanoscale: optical and photothermal properties and some applications in imaging, sensing, biology, and medicine." *Accounts of chemical research* 41.12 (2008): 1578-1586.
6. Gupta, Banshi D., Vivek Semwal, and Anisha Pathak. "Nanotechnology-based fiber-optic chemical and biosensors." *Nano-optics: fundamentals, experimental methods, and applications* (2020): 163.
7. Shipway, Andrew N., Eugenii Katz, and Itamar Willner. "Nanoparticle arrays on surfaces for electronic, optical, and sensor applications." *ChemPhysChem* 1.1 (2000): 18-52.
8. Kalantar-Zadeh, Kourosh, and Benjamin Fry. *Inorganic nanotechnology enabled sensors*. Springer US, 2008.
9. Lee, Seokhyeong, et al. "Programmable black phosphorus image sensor for broadband optoelectronic edge computing." *Nature communications* 13.1 (2022): 1485.
10. Ungureanu, Constantin, et al. "Discrete dipole approximation simulations of gold nanorod optical properties: Choice of input parameters and comparison with experiment." *Journal of Applied Physics* 105.10 (2009).
11. Yao, Jun, et al. "Upconversion luminescence nanomaterials: A versatile platform for imaging, sensing, and therapy." *Talanta* 208 (2020): 120157.
12. Wang, Lu, Morteza Hasanzadeh Kafshgari, and Michel Meunier. "Optical properties and applications of plasmonic-metal nanoparticles." *Advanced Functional Materials* 30.51 (2020): 2005400.